Supporting Information

Vertical growth of SnS_2 nanobelt arrays on $CuSbS_2$ nanosheets for enhanced photocatalytic reduction of CO_2

Wenhao Li,[a] Quanlong Xu,*[a] Wei Chen,[a] Faliang Gou,[b] Shujing Zhou,[c] Jinjing Li,[c] Chenze Qi [bc] and De-Kun Ma *[b]

[a] *Zhejiang Key Laboratory of Carbon Materials, Wenzhou University, Wenzhou 325027, China*

[b] *Zhejiang Key Laboratory of Alternative Technologies for Fine Chemicals Process, Shaoxing University, Shaoxing 312000, China*

[c] *School of Pharmacy, Jiamusi University, Jiamusi 154007, China.*

**Email addresses: xuql@wzu.edu.cn; dkma@usx.edu.cn*

Experimental Section

1. Chemicals and Purity

Cuprous chloride (CuCl, AR), Antimony trichloride ($SbCl_3$, AR, 99%), Tin chloride pentahydrate ($SnCl_4 \cdot 5H_2O$, AR, 99.0%), Thiourea (CH_4N_2S, ACS, ≥99.0%), Thioacetamide (C_2H_5NS, AR, 99%), Oleylamine ($C_{18}H_{37}N$, C_{18}: 80-90%), Sodium sulfafe (Na_2SO_4, AR), and Ethanol absolute (C_2H_6O, AR, 95%) were purchased from Aladdin Shanghai Co. Ltd. Acetone was purchased from Zhejiang Zhongxing Chemical Co.Ltd. All the chemicals were used as received unless otherwise stated.

2.1 Synthesis of $CuSbS_2$ nanosheets.

In a typical synthesis, CuCl (0.5 mmol), $SbCl_3$ (0.5 mmol), and CH_4N_2S (1.5 mmol) were dissolved in 10 mL of oleyamine at a molar ratio of 1 : 1 : 3 and backfilled with nitrogen at 80 °C. Then, the solution was transferred into a 50 mL Teflon-lined stainless steel autoclave and heated at 240 °C for 1 h. The resultant products were washed with acetone for four times and then dried at 60 °C in oven.

2.2 Synthesis of $SnS_2 \perp CuSbS_2$ heterostructures

To the synthesis of $SnS_2 \perp CuSbS_2$ heterostructures, 0.25 mmol of as-synthesized $CuSbS_2$ nanosheets were dispersed into 10 mL of ethanol absolute under stirring (A solution). 0.125 mmol of $SnCl_4 \cdot 5H_2O$ and 0.25 mmol CH_4N_2S were added into another 10 mL of ethanol (B solution). After 10 minutes' agitation, A solution was put into B solution. After 30 minutes' stirring, the solution was transferred into a 50 mL Teflon-lined stainless steel autoclave and heated at 180 °C for 12 h. The resultant products were washed with ultrapure water, acetone, and ethanol absolute for three times. Then dried at 60 °C in oven.

2.3 Synthesis of SnS_2 nanosheets

The synthetic conditions of SnS_2 nanosheets are similar to those of $SnS_2 \perp CuSbS_2$ heterostructures except without introduction of $CuSbS_2$ nanosheets.

2.4 Preparation of photoelectrodes

The preparation processes of $CuSbS_2$ and SnS_2 photoelectrodes are similar. In a typical process, a piece of F-doped tin oxide (FTO) glass (1 cm × 2 cm) was ultrasonically cleaned three times through successive exposure to H_2O_2 (30%), ethanol, and ultrapure water. Then, 10 mg of the sample was dispersed in 1 mL of ethylene glycol by sonification. 50 μL of the dispersion was evenly coated on the glass via direct drop-casting. Subsequently, the sample-coated glass was dried at 80 °C under vacuum, annealed in Ar at 180 °C for 2 h, and then cooled to room temperature.

Characterization

X-ray diffraction (XRD, D8 Advance) was used to characterize the crystal phases of the products. Field emission scanning electron microscopy (FE-SEM, Nova NanoSEM 200), HRTEM and HAADF-STEM (JEOL ARM-200F), and EDX analysis (FEI Talos F200X TEM) were used to study the morphology, interfacial structure, and composition of the samples. UV–visible absorption spectra (UV–vis, Shimadzu 2450) obtained by a diffuse reflectance spectroscopy with $BaSO_4$ as the reference for studying the optical responsive range of the samples. X-ray photoelectron spectroscopy (XPS, Escalab 250Xi, Thermo Scientific) using Al Kα radiation (hν = 1486.6 eV) as excitation, and ultraviolet photoelectron spectroscopy (UPS) attached to the XPS system was used to analyze the

composition and chemical states of the prepared samples. N_2 adsorption-desorption isothermals were recorded on ASAP2020 HD88 instrument, which were used to measure specific surface area of the samples. 0.1 g of sample was added into the sample tube and then vacuumed, activated at 200 °C for 8 h. After the sample cooled to room temperature, N_2 adsorption-desorption curve measurement was started. PL spectra were measured on a Fluoromax-4 spectrofluorometer (HORIBA JobinYvon Inc.) under an excitation wavelength of 400 nm at room temperature. The electrochemical impendance spectra (EIS) were carried out at 2 V versus reversible hydrogen electrode with an amplitude of 5 mV in a frequency range from 0.1 MHz to 0.1 Hz in 0.5 M Na_2SO_4 electrolyte in the dark and under light irradiation (AM1.5G, 100 $mWcm^{-2}$), respectively. Photocurrent – time and photocurrent – potential curves of the photoelectrodes were performed in 0.5 M Na_2SO_4 aqueous electrolyte under chopped light illumination (AM 1.5 G, 100 mW cm^{-2}). The gaseous products from the photocatalytic CO_2RR were analyzed by gas chromatograph (Fuli GC9790).

Photocatalytic CO_2RR

The photocatalytic CO_2RR of the samples was evaluated in a closed reaction device containing a quartz container. In a typical process, SnS_2⊥ $CuSbS_2$ heterostructures (10 mg) were dispersed into the mixed solvent of H_2O:TEOA = 10:1 (vol/vol). Then the reaction setup was alternately vacuum-degassed and purged with CO_2 for three times. The final pressure of the reactor containing CO_2 gas reaches one atmosphere. The reaction solution was stirred and irradiated under a 300 W Xenon lamp equipped with a cut-off filter ($\lambda > 420$ nm). The temperature was controlled at 15° C by circulating cooling water and heater. The gaseous products were analysized by a gas chromatography. To evaluate stability of the photocatalysts, the photocatalytic CO_2RR was performed for 6 h at first. And then, the photocatalysts were separated from the reaction solutions by centrifugation. After washed and dried, they were re-dispersed into fresh reaction solutions to perform photocatalytic CO_2RR. The process was repeated four times and the gas yield was recorded.

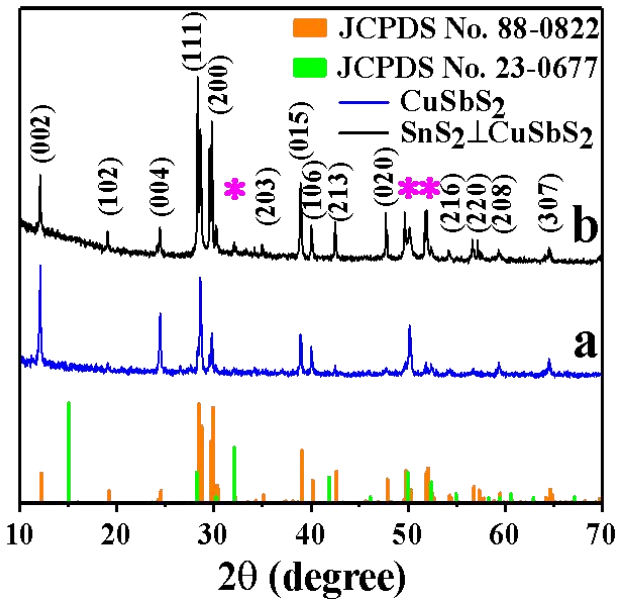

Fig. S1 XRD patterns of the as-synthesized $CuSbS_2$ nanosheets (a) and SnS_2 ⊥ $CuSbS_2$ heterostructures (b).

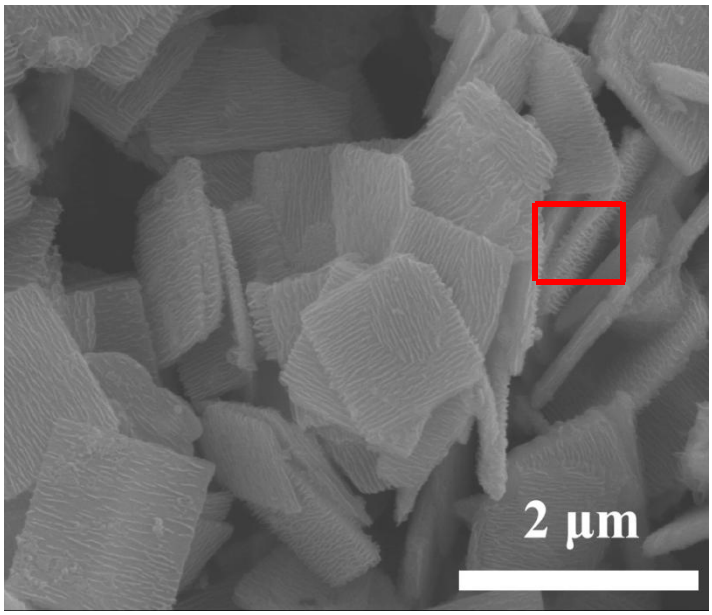

Fig. S2 FE-SEM image of SnS_2 ⊥ $CuSbS_2$ heterostructures.

As seen from red rectangular frame, SnS_2 nanobelt arrays were grown on both the top and bottom of $CuSbS_2$ nanosheets.

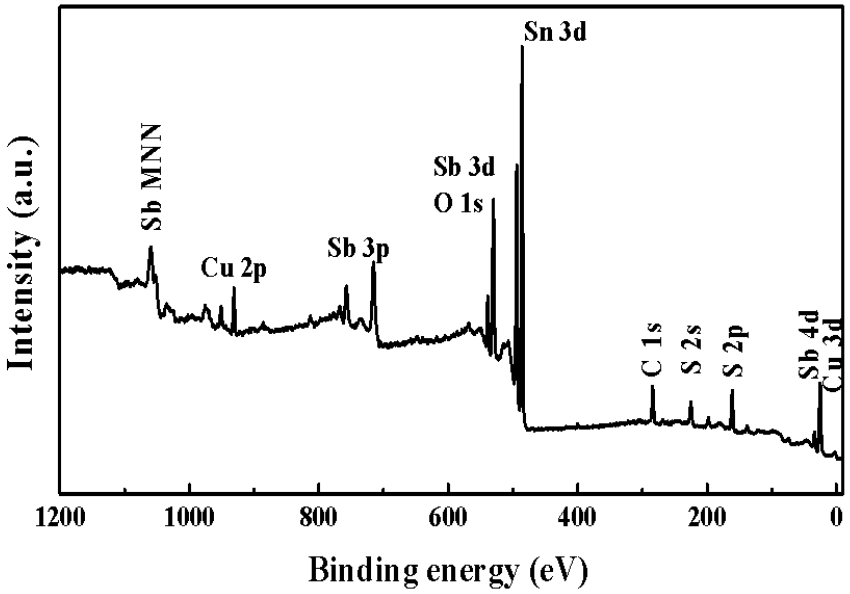

Fig. S3 XPS survey spectrum of $SnS_2 \perp CuSbS_2$ heterostructures.

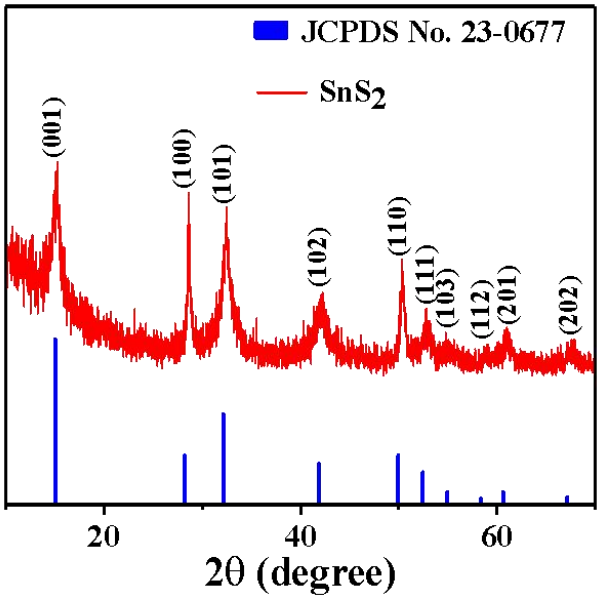

Fig. S4 XRD pattern of the as-synthesized SnS_2 nanosheet.

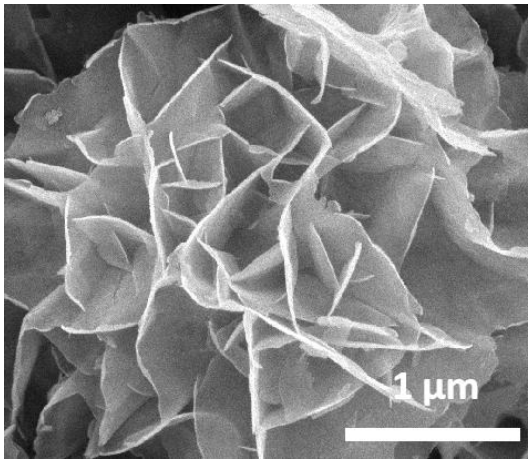

Fig. S5 FE-SEM image of the as-synthesized SnS_2 nanosheet.

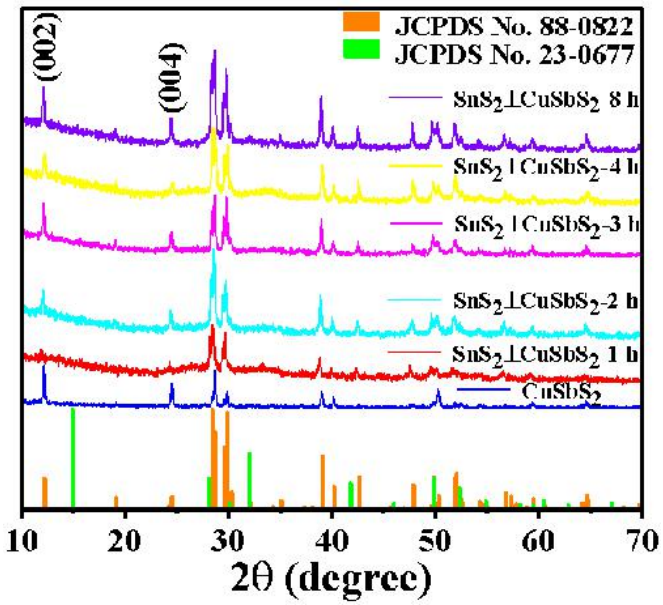

Fig. S6 Time-dependent XRD patterns of the intermediate products obtained at different reaction time.

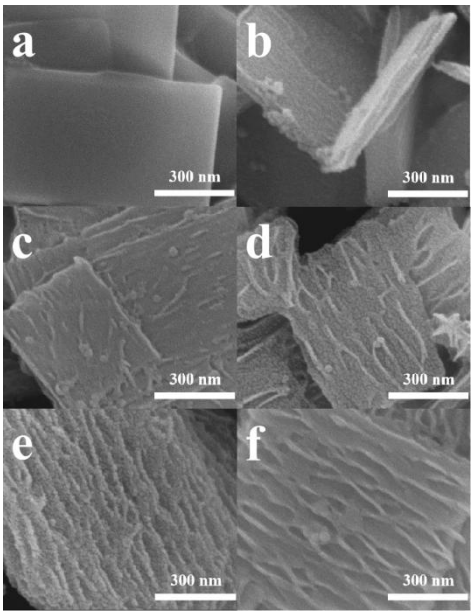

Fig. S7 Time-dependent FE-SEM images of the intermediate products obtained at different reaction time: 0 h (a), 1 h (b), 2 h (c), 3 h (d), 4 h (e), and 8 h (f).

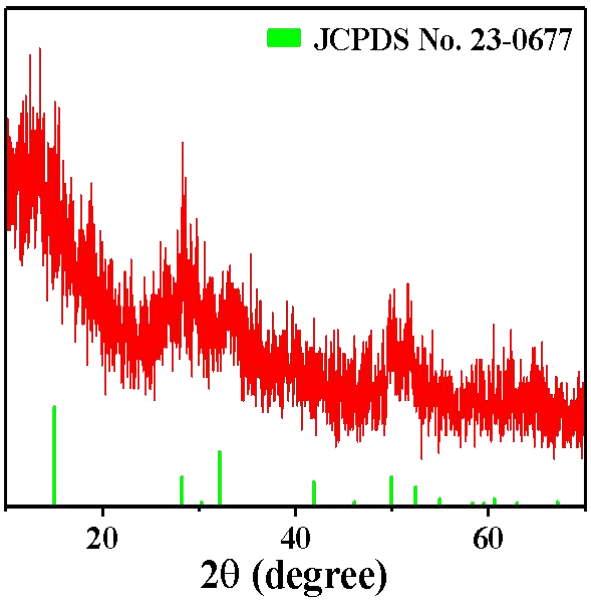

Fig. S8 XRD pattern of the products synthesized at increased molar ratio of $SnCl_4$ to $CuSbS_2$.

When the molar ratio of $SnCl_4$ to $CuSbS_2$ increased from 1:2 to 4:1, keeping other reaction conditions unchanged, as seen from Fig. S8, XRD diffraction peaks of $CuSbS_2$ disappeared and only

diffraction peaks of SnS_2 were observed. That is to say, $CuSbS_2$ could be converted to SnS_2 in the present reaction system.

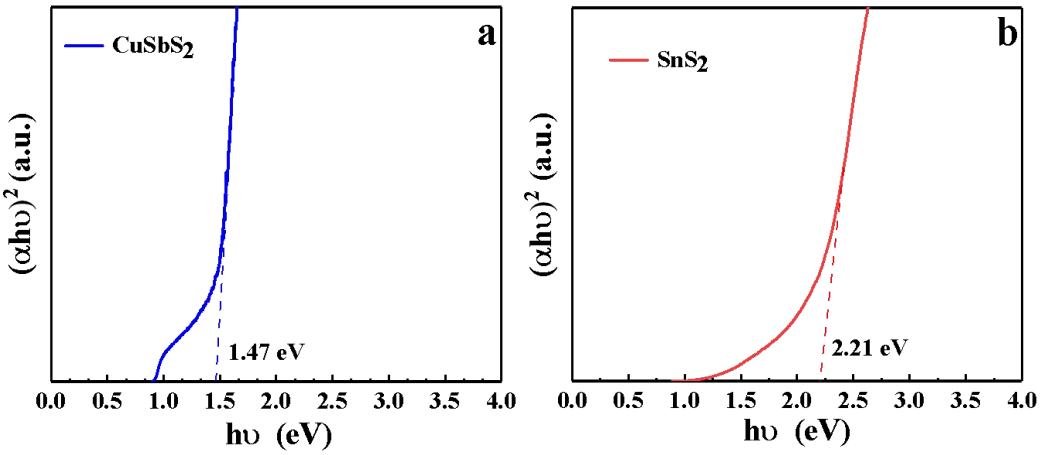

Fig. S9 $(\alpha h\nu)^2$ versus $h\nu$ curves of $CuSbS_2$ nanosheets (a) and SnS_2 nanosheets (b).

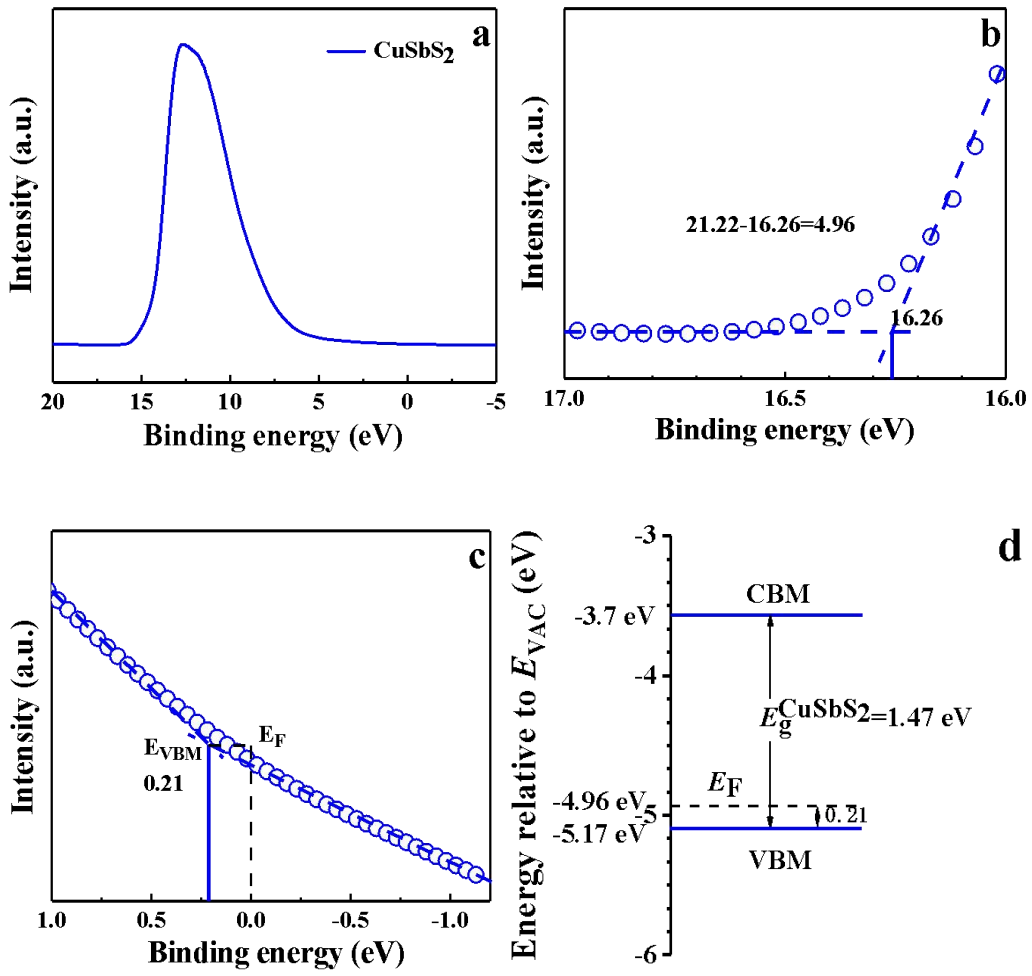

Fig. S10 UPS spectrum of $CuSbS_2$ (a). The secondary electron cut-off energy of 16.26 eV (b), which is determined from the intersection of the linear portion of spectrum and the baseline. The determination of E_{VBM} (c). Schematic energy band positions of $CuSbS_2$ with respect to the vacuum level (d).

.

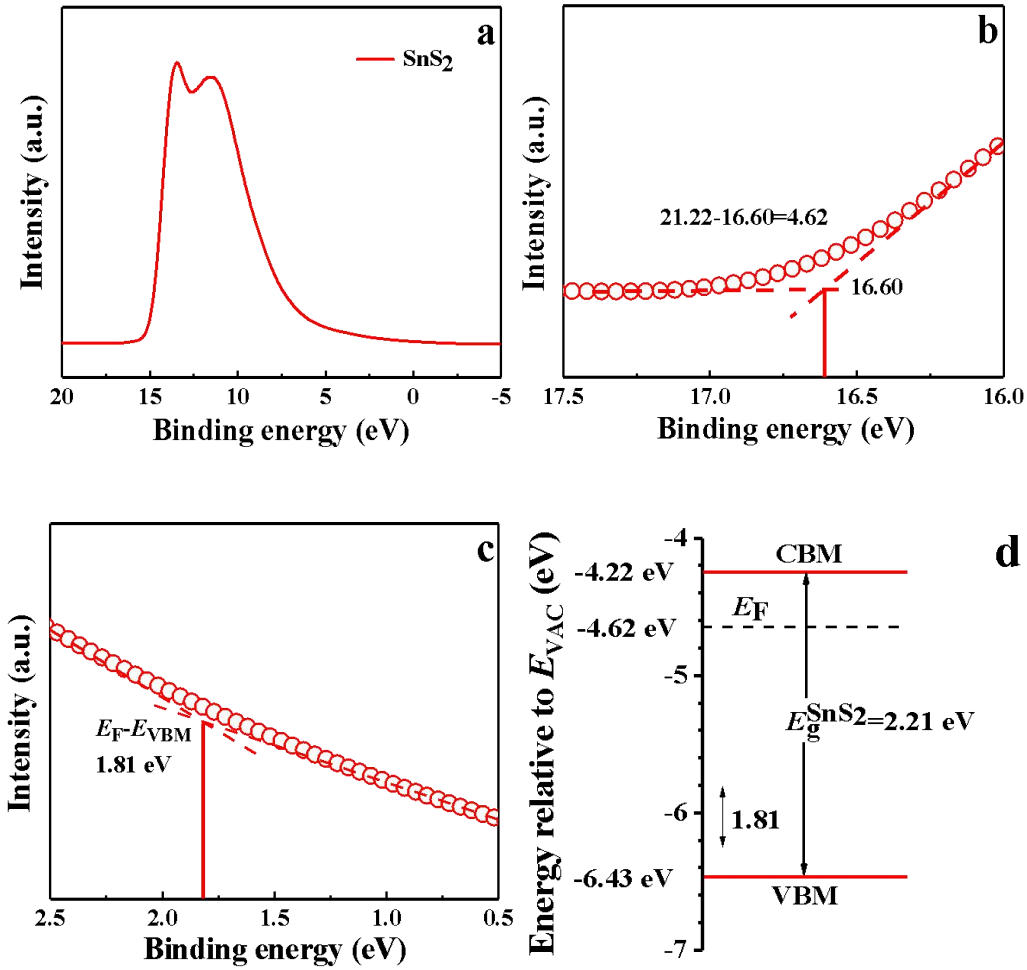

Fig. S11 UPS spectrum of SnS_2 (a). The secondary electron cut-off energy of 16.60 eV (b), which is determined from the intersection of the linear portion of spectrum and the baseline. The determination of E_{VBM} (c). Schematic energy band positions of SnS_2 with respect to the vacuum level (d).

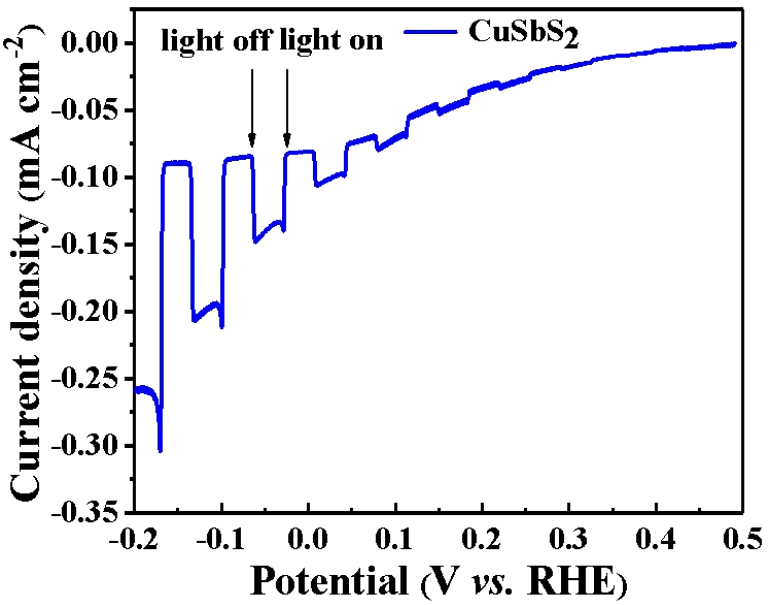

Fig. S12 Photocurrent–potential curve of $CuSbS_2$ nanosheets under chopped light illumination (AM 1.5 G, 100 mW cm^{-2}).

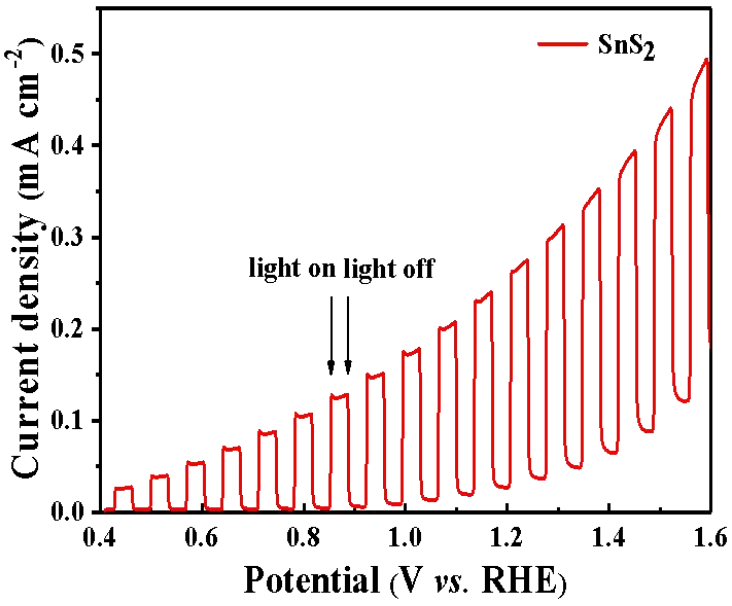

Fig. S13 Photocurrent–potential curve of SnS_2 nanosheets under chopped light illumination (AM 1.5 G, 100 mW cm^{-2}).

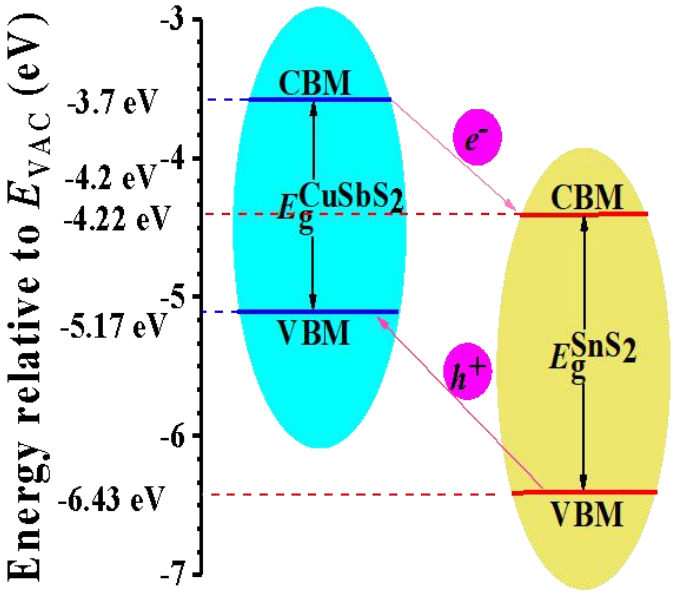

Fig. S14 Schematic energy band diagram of SnS_2 nanoshees and $CuSbS_2$ nanosheets and separation process of photogenerated carriers.

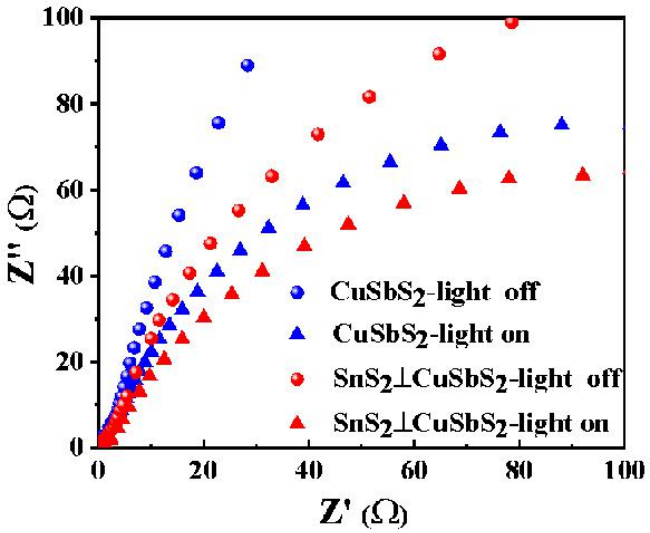

Fig. S15 Nyquist plots of $CuSbS_2$ nanosheets and $SnS_2 \perp$ $CuSbS_2$ heterostructures obtained at an applied potential of 2 V vs. RHE performed in the dark and under light illumination (AM 1.5 G, 100 mW cm^{-2}).

As shown in Fig. S15, in both instances, namely, under light irradiation and in the dark, $SnS_2 \perp CuSbS_2$ heterostructures showed smaller resistance of charge transfer than individual $CuSbS_2$. This result showed that the heterostructure promoted the transfer of charge.

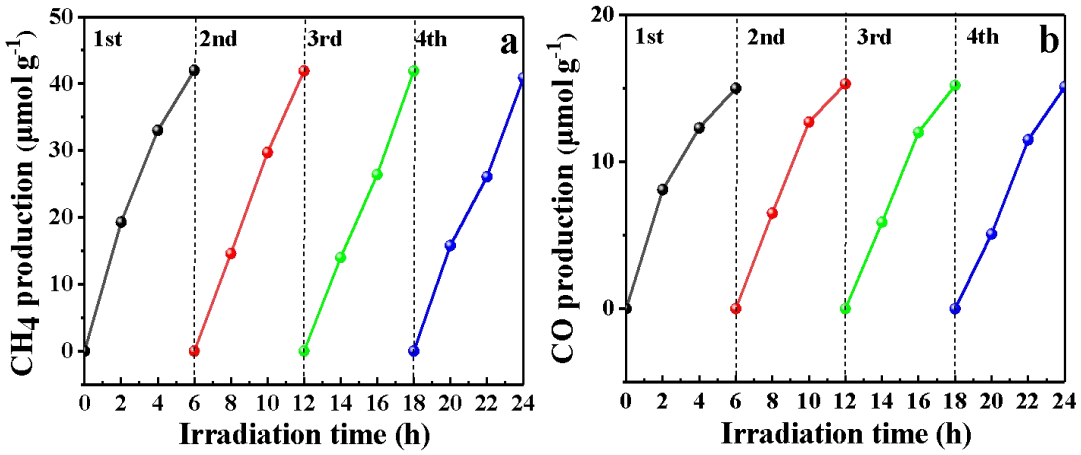

Fig. S16 The stability of $SnS_2 \perp CuSbS_2$ heterostructures after 4 cycles photocatalytic CO_2RR.

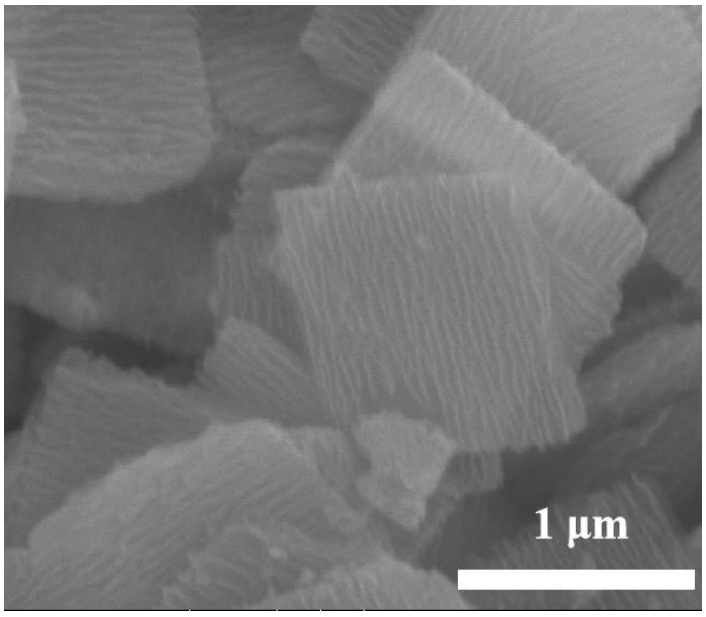

Fig. S17 FESEM image of the sample after four times photocatalytic CO_2RR.

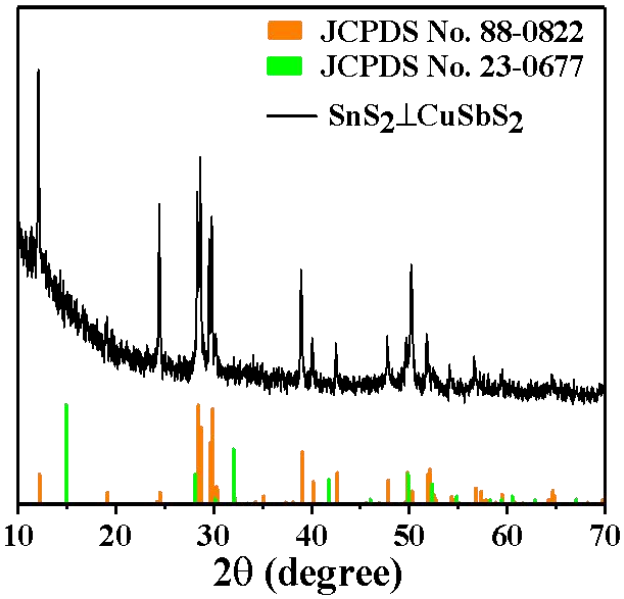

Fig. S18 XRD pattern of the sample after four times photocatalytic CO_2RR.